



**POLITECNICO**  
**MILANO 1863**

**SCUOLA DI INGEGNERIA INDUSTRIALE  
E DELL'INFORMAZIONE**

EXECUTIVE SUMMARY OF THE THESIS

## A reduced model for the flow in the human nose

LAUREA MAGISTRALE IN AERONAUTICAL ENGINEERING - INGEGNERIA AERONAUTICA

**Author: ANGELO RAIMONDO FAVERO**

**Advisor: PROF. MAURIZIO QUADRIO**

**Co-advisor: DOTT. EMANUELE GALLORINI**

**Academic year: 2023-2024**

### 1. Introduction

Nasal defects and pathologies can lead to respiratory diseases. For their evaluation, the OpenNOSE project has the objective of developing an open-source diagnostic methodology that integrates Computational and Experimental Fluid Dynamics with medical challenges like nasal surgery. This aims to assist healthcare professionals in diagnosing and treating patients with conditions affecting their quality of life.

In this thesis, is presented a CFD program, written in the CPL environment [1] by professor Paolo Luchini, based on a simplified model of a flow in Stokes regime, for the computation of the airflow in the nasal cavities. This method can result to be useful as it has been seen that for the purpose of medical evaluation, often, really accurate methods are not needed [2]. This program simulates airflow on real geometries extracted from CT scans and computes the results extremely fast. For each patient the computational time needed is of a few seconds. The primary aim is to create a tool for real-time diagnosis and surgical planning. A significant part of the thesis focuses on the program's functionality and results obtained. Additionally, an automated process is introduced for solving the problem and generating results on a large database of

patients, with the aim of finding correlations between CFD results and anatomical pathologies identified by ENT specialists. The pathologies studied are turbinate hypertrophies and septal deviations.

### 2. Governing equations and numerical solution

The governing equations of the system coming from the conservation of mass, momentum and energy are:

$$\begin{cases} \nabla \cdot \mathbf{u} = 0 & (1a) \\ \mathbf{u} = -\mathcal{K} \cdot \nabla P & (1b) \\ \nabla \cdot (k_T \nabla T) + \mathbf{u} \cdot \nabla T = 0 & (1c) \end{cases}$$

The equations of momentum (1b), are written in the form of Darcy's law, which is the governing equation for flow in porous materials.  $\mathcal{K}$  represents the hydraulic conductivity and it is in the form of a tensor to take into account the directional variability of the quantity.

#### 2.1. Hele-Shaw flow

For the computation of the hydraulic conductivity in the nose airways, will be used a model based on Hele-Shaw flow. Hele-Shaw is a flow taking place between two parallel flat plates sep-

arated by a really narrow gap (Fig. 1). The condition to be verified for this kind of flow is:

$$Re \frac{h}{l} \ll 1 \quad (2)$$

Where  $Re = uh/\nu$  is the Reynolds number and  $l$  is the characteristic length scale in directions parallel to the plate.

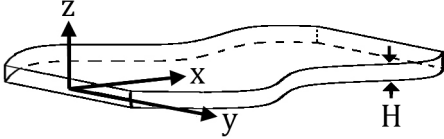


Figure 1: Hele-Shaw configuration

The non-null velocity components for this kind of flow (Eqs. 3) can be described by Darcy's law, with the hydraulic conductivity  $K$  constant on the  $x$  and  $y$  directions and varying along the width of the channel (Eq. 4):

$$\begin{cases} v_x = -\frac{1}{2} \frac{\partial p}{\partial x} z(h-z) & (3a) \\ v_y = -\frac{1}{2} \frac{\partial p}{\partial y} z(h-z) & (3b) \\ v_z = 0 & (3c) \end{cases}$$

$$K(z) = \frac{z}{2}(h-z) \quad (4)$$

For this kind of flow it is possible to consider the depth averaged version of any quantity. The depth averaged conductivity is:

$$\langle K \rangle = \frac{h^2}{12} \quad (5)$$

## 2.2. tp3d

The code used for the computation of the flow inside the nose is called **tp3d** and is developed in Compiler and Programming Language (CPL). It implements a reduced model for the flow of air in the nasal cavities as that of a fluid through a three dimensional anisotropic porous medium. The main steps performed by the program can be summarized as:

- Geometry extraction from the CT scans
- Computation of the conductivity
- Computation of the pressure field with the governing equations of mass and momentum

- Obtaining the flow rates in the nostrils and the throat, and the fields of velocity and energy dissipation
- Computation of temperature field including the governing equation for energy

**Geometry Extraction:** Before commencing computations, a method is implemented to extract the airway geometry from the entire head tomography of patients. This is achieved using a logical function based on voxel radiodensity and a specified threshold value. Additionally, to facilitate comparison across all patients, the distance in millimeters from the tip of the nose to the throat is delineated and standardized for each patient.

**Computation of Conductivity:** The practical approach to computing hydraulic conductivity in the airway involves evaluating the definite integral of conductivity between the solid boundaries for each voxel. This integral is derived from either Eq. 4, as illustrated in Fig. 2, or Eq. 5.

To accomplish this, distances from the solid boundaries in the three principal directions are calculated for each element. Subroutines such as *STARLINE* and *UPDPOS* are utilized for this purpose, with the latter employing interpolation techniques to accurately determine the position of the solid-fluid interface.

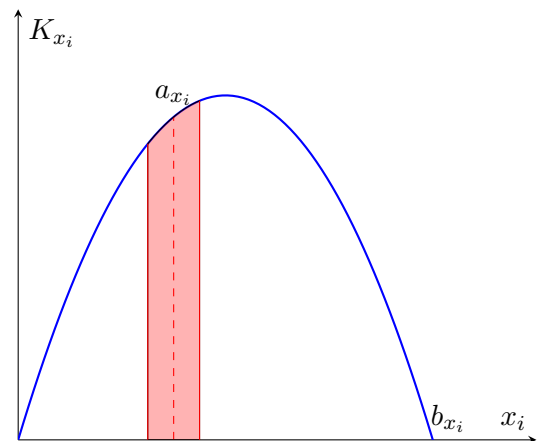


Figure 2: Definite integral visualization.

This way are obtained the three directional contributions to hydraulic conductivity. Taking their harmonic sum (Eq. 6) it is computed a comprehensive value of conductivity in each voxel.

$$K(i) = \frac{K_x(i)K_y(i)K_z(i)}{K_x(i)K_y(i) + K_y(i)K_z(i) + K_x(i)K_z(i)} \quad (6)$$

$$i = [i_x, i_y, i_z]$$

To consider the different directional components of permeability, it is sufficient to compute the mean between the conductivity in a voxel and the adjacent one.

**Pressure field:** For the computation of the field of pressure it is necessary to impose the initial conditions, with pressure  $P = 1$  [Pa] at the inlet and  $P = 0$  [Pa] at the outlet. All the active points are initialized with unitary value of pressure and the barrier voxels are assigned  $P = -0.199$  [Pa]. Exploiting the values of permeability calculated in the precedent step, it is possible to compute numerically the pressure field. In this method, is evaluated the balance of the volumetric flow rates on each finite volume. To perform this task, it is considered a solution that respects the conservation of mass (Eq. 1a) and momentum (Eq. 1b) in every element of the system.

For the sake of a fast numerical convergence is employed a multigrid method, in which for the smoothing is used a red-black Successive Over-Relaxation (SOR) method, with the objective of an efficient parallelization. The solution is considered converged when an imposed value of residual is reached.

**Velocity and volumetric flow rates:** With the values of pressure and conductivity, it is possible to compute the air velocity field and flow rates in the nostrils and the throat. This is done exploiting the conservation of momentum (Eq. 1b). The flow of air at the interface of two voxels is:

$$Q(i, d) = \frac{\frac{K(i)+K(i+d)}{2} \left( P(i+d) - P(i) \right)}{\Delta d} A_n \quad (7)$$

- $i = (i_x, i_y, i_z)$  denotes the index vector of the voxel considered.
- $d$  represents the directional unit displacements  $dx = (1, 0, 0)$ ,  $dy = (0, 1, 0)$ , and

$dz = (0, 0, 1)$ , corresponding to each spatial dimension.

- $\Delta d$  refers to the voxel dimension in the direction of  $d$ .
- $A_n$  is the area of the interface of the two elements.

When printing the results, the volumetric flow rates computed in the nostrils and in the throat are normalized, taking unitary flow in the throat.

**Temperature:** The temperature at each point in the volume is computed using a method similar to that used for the pressure field. In the model, the temperature is considered dimensionless. The inlet and outlet temperatures are set to 1 and 0, respectively. The boundary temperature for all barrier voxels is set to  $T_B = 10^{-4}$ . All active points are initialized with a temperature  $T(i_x, i_y, i_z) = P(i_x, i_y, i_z)/\Delta P$ . The numerical solution is obtained using Eq. 1c without applying multigrid and SOR, as convergence is not an issue. From the computed temperature field, the mean temperature in the throat,  $T_{th}$ , is also determined.

## 3. Applications of the code

### 3.1. Test on simple geometry

To verify the proper functionality and correct usage of the **tp3d** code, a test was conducted on the geometry of a straight cylinder. The theoretical solution for Stokes flow in this geometry is given by the Hagen-Poiseuille equation. The results obtained from the test are compared with the theoretical solutions in terms of volumetric flow rate across a section of the cylinder, with varying radius values.

The results from the theoretical and computational methods are comparable, as shown in Fig. 3. However, there is still a difference between the numerical and theoretical results that needs to be investigated. This discrepancy may be related to the boundary definition. Nonetheless, it is considered acceptable for the purposes of this work.

### 3.2. Comparison with DNS

The results obtained are also compared with the ones coming from a Direct Numerical Simulation (DNS), that was performed for this purpose on a selected patient. The flow distribution between

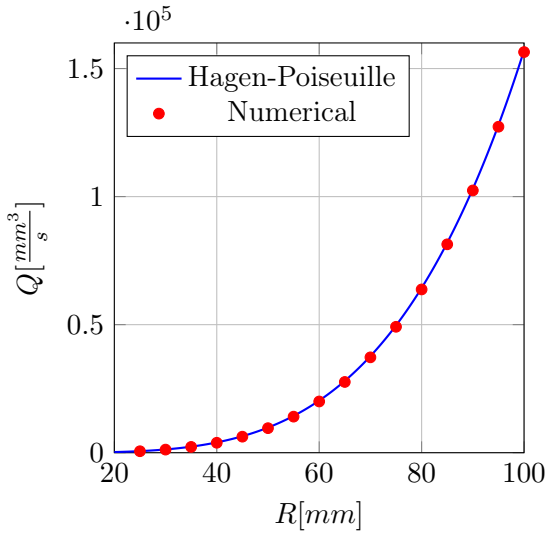


Figure 3: Results for the volumetric flow rate at various radii.

Table 1: Flow distribution in the two nostrils.

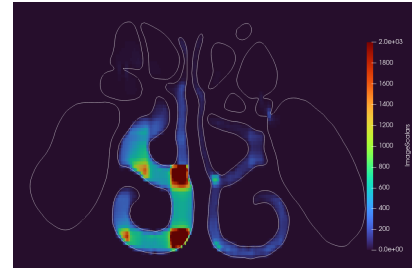
Flow rate	tp3d	DNS
$Q_{RN}\%$	90.6%	85.3%
$Q_{LN}\%$	9.4%	14.7%

the two nostrils computed with the two methods is compared in Table 1.

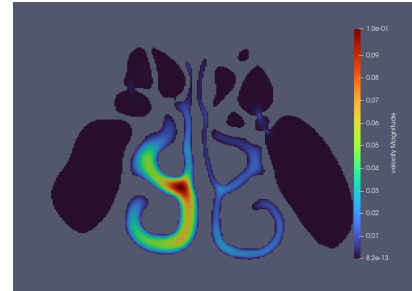
The outcomes show that, **tp3d** tends to overestimate the flow rate in the right nostril compared to the DNS solution. The different flow distribution can be associated with the high velocity magnitude seen in the lower air passage for **tp3d**, which is absent in the DNS solution (Fig. 4). This effect is probably linked with how the hydraulic conductivity is computed, as a similar distribution is seen also in the permeability field (Fig. 5).

### 3.3. Effect of the radiodensity threshold imposed

The selection of the value of radiodensity threshold used to extract the geometry of the airway can have a relevant influence on the numerical results obtained [3]. For this reason, the pressure drop between the external air and the throat ( $\Delta P$ ), as well as the mean temperature in the throat ( $T_{th}$ ), are calculated for different imposed thresholds for the same patient. The outcomes of this study are reported in Fig. 6, together with the results obtained applying the same procedure, but turning off the correction on the in-



(a) tp3d



(b) DNS

Figure 4: Coronal view of the velocity magnitude field

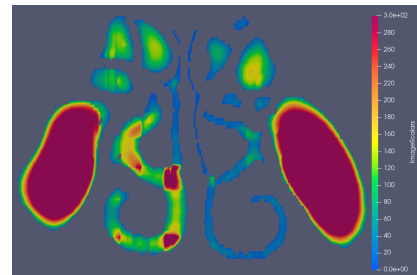


Figure 5: Coronal view of permeability distribution

terpolation of the boundary. It can be observed that the value of  $\Delta P$  decreases monotonically increasing the radiodensity threshold, when the correction is not applied. While, when applying the correction, between  $-300$  HU and  $-500$  HU  $\Delta P$  is nearly constant, otherwise it increases.

### 3.4. Correlation between pathologies and results

The values of  $\Delta P$  and  $T_{th}$  calculated for each patient in the database are associated with the respective pathologies. From Table 2 and Fig. 7, several general observations can be made. Patients with turbinate hypertrophies exhibit higher  $\Delta P$  and lower  $T_{th}$ , while septal deviations seem to have a lower impact on overall resistance. To convey the relationship between pressure and temperature, results are displayed

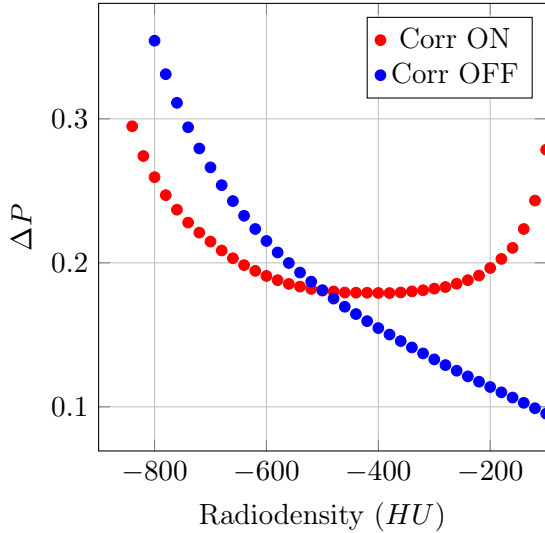


Figure 6:  $\Delta P$  patient 0002 for different threshold values.

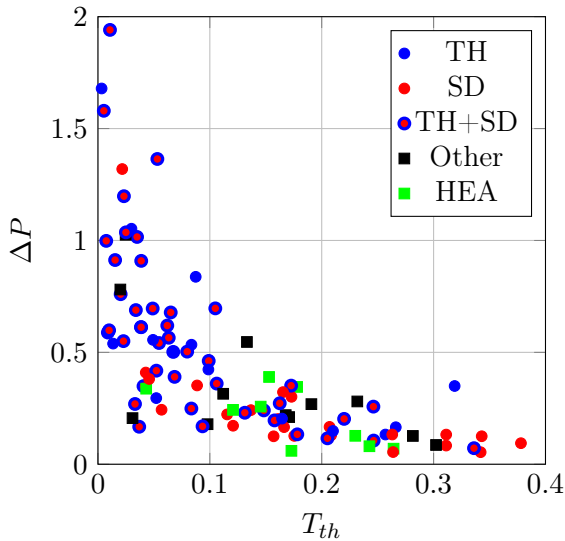


Figure 7:  $\Delta P - T_{th}$  plots.

as in Fig. 7, demonstrating a general trend where higher pressure differences are associated with greater changes in temperature.

- TH: Turbinate pathologies.
- SD: Septal deviation.
- TH+SD: Both pathologies.
- Other: Other pathologies
- HEA: Healthy.

Septal deviations affect the most the distribution of the flow in the nostrils. Considering all the patients with a septal deviation to the right, the mean value of air flow percentage in the right nostril is 35.3 %, while for septal deviations towards the left, the flow in the right nostril con-

Table 2: Mean values.

Label	Mean $\Delta P$	Mean $T_{th}$
TH	0.5931	0.1262
SD	0.2815	0.1658
TH+SD	0.5879	0.1066
HEA	0.2050	0.2184

stitutes the 64.5 % of the total.

## 4. Conclusions

This thesis involved a preliminary approach to the code **tp3d**, including extensive work and testing, demonstrating its potential for fluid dynamics computations in a realistic nose geometry. It has been possible to run the code on good part of the entire database, with a very short computational time, obtaining significant numerical results that showed some correlations with the pathologies of the patients. Even if this first approach on the code is to be considered positive there is still a lot of work to be done to test and possibly improve it. The comparison with the results coming from the DNS shows that there are still important differences between the two flows computed. A limitation of the code resides in the kind of flow studied, in fact the approximation to a Stokes flow for the airflow inside the nose can be considered reliable only for extremely low inspiration rates. As it has been verified that, in general, for normal inspiration, the flow cannot be fully described with a laminar model [4]. It is necessary to underline that the purpose of using **tp3d**, is not to find results that model correctly every feature of the flow inside the nose. The main objective is for it to pick up important features of the airway that may be useful to realize diagnoses and surgery. With this purpose another part of the code is being developed that includes an optimization on the geometry of the airway with an adjoint method.

## 5. Bibliography

- [1] P. Luchini. *Introducing CPL*. Nov. 2021. arXiv: [2012.12143 \[physics\]](https://arxiv.org/abs/2012.12143) (cit. on p. 1).
- [2] H. Calmet, K. Inthavong, H. Owen, D. Dosimont, O. Lehmkuhl, G. Houzeaux, and M. Vázquez. “Computational Modelling of

- Nasal Respiratory Flow”. In: *Computer Methods in Biomechanics and Biomedical Engineering* 24.4 (Mar. 12, 2021), pp. 440–458. DOI: [10 . 1080 / 10255842 . 2020 . 1833865](https://doi.org/10.1080/10255842.2020.1833865) (cit. on p. 1).
- [3] M. Quadrio, C. Pipolo, S. Corti, F. Messina, C. Pesci, A. Saibene, S. Zampini, and G. Felisati. “Effect of CT Resolution and Radiodensity Threshold on the CFD Evaluation of Nasal Airflow”. In: *Medical & Biological Engineering & Computing* 54 (2016), pp. 411–419. DOI: [10 . 1007 / s11517 - 015 - 1325 - 4](https://doi.org/10.1007/s11517-015-1325-4) (cit. on p. 4).
- [4] D. Doorly, D. Taylor, A. Gambaruto, R. Schroter, and N. Tolley. “Nasal Architecture: Form and Flow”. In: *Philosophical Transaction of the Royal Society* 366 (2008), pp. 3225–3246. DOI: [10.1098/rsta.2008.0083](https://doi.org/10.1098/rsta.2008.0083) (cit. on p. 5).